Available online at www.sciencedirect.com
ScienceDirect
Advances in Space Research 39 (2007) 1483–1490
ADVANCES IN SPACE RESEARCH (a COSPAR publication)
www.elsevier.com/locate/asr

# The multi-wavelength study of the effect of energetic particle beams on the chromospheric emission in the 25th July 2004 solar flare

V.V. Zharkova [a,*], L.K. Kashapova [b], S.N. Chornogor [c], O.V. Andriyenko [c,d]

[a] *The School of Informatics, University of Bradford, Richmond Road, Bradford, West Yorkshire BD7 1DP, UK*
[b] *Radio-astrophysical Department, Institute of Solar-Terrestrial Physics, Lermontov St., 126, P.O. 4026, Irkutsk 664033, Russia*
[c] *Main Astronomical Observatory, NASU, 27 Akademika Zabolotnoho St., 03680 Kyiv, Ukraine*
[d] *IC AMER, NASU, 27 Akademika Zabolotnoho St., 03680 Kyiv, Ukraine*

Received 7 November 2006; received in revised form 21 March 2007; accepted 3 April 2007

**Abstract**

We present the multi-wavelength study of short-term variations of Hα line emission located in multiple kernels on the both sides from magnetic neutral line in the 25th July 2004 solar flare observed by VTT (Tenerife). The HXR and Hα emission in the kernels 1 and 3 is close spatially and temporally while in kernels 4 and 7 there is only delayed Hα emission observed tens seconds after HXR in the kernels 1 and 3. The locations of Hα kernels 1, 3, 4 and 7 are on the opposite sides from the magnetic neutral line. The temporal variations of Hα emission in kernels 1 and 3 coincide within 5 s with the HXR photon emission. The latter is found to have double power law photon spectra, which were corrected to a single power law with the turning point technique accounting for Ohmic losses and collisions. The Hα emission is fit by full non-LTE simulations in an atmosphere heated by an electron beam with the parameters derived from the HXR emission. The combination of radiative, thermal and non-thermal mechanisms of excitation and ionization of hydrogen atoms is considered. The temporal evolution of simulated Hα emission in the kernel 3 fits rather well the two observed intensity increases: the first at the flare onset (13:38:39–13:39:30 UT) caused by pure non-thermal excitation by beam electrons and the second one appearing after 13:40:00 UT because of a hydrodynamic heating. The observed close temporal correlation or delay of Hα emission with HXR emission points out to the precipitation either of electron (kernels 1 and 3) or protons (4 and 7).


*Keywords:* Solar flares; Energy transport; Particle beams; Hydrodynamic response; Non-thermal excitation

## 1. Introduction

Rapid variations of the Hα line intensity and its correlation with HXR flux during the impulsive phase of chromospheric flares were reported by many authors, e.g., Trottet et al. (2000). Also a comparison of the spatial distribution of HXR sources with Hα flare kernels showed that during the evolution of flare ribbons many Hα kernels brighten simultaneously with the HXR emission (Asai et al., 2002).

Fast temporal fluctuations of both HXR and optical emissions are usually attributed to the propagation of the accelerated particle beams from the upper to lower atmospheric layers and energy dissipation in chromosphere and photosphere (see for a review Heinzel, 2003). The HXR sources are often located on the external edges of the Hα emission and connected with the chromospheric plasma heated by the non-thermal electrons (Kašparová et al., 2005a,b).

However, the fast changes of Hα intensity are often placed not only inside the HXR sources, as expected if they are the signatures of the chromospheric response to the electron bombardment, but appear outside and far away from them, sometimes on the opposite side from the magnetic neutral line (Asai et al., 2002). This can indicate that a

* Corresponding author.
*E-mail addresses:* v.v.zharkova@Bradford.ac.uk, v.v.zharkova@brad.ac.uk (V.V. Zharkova), lkk@iszf.irk.ru (L.K. Kashapova), chornog@MAO.Kiev.ua (S.N. Chornogor), olexa@MAO.Kiev.ua (O.V. Andriyenko).

0273-1177/$30 © 2007 COSPAR. Published by Elsevier Ltd. All rights reserved.
doi:10.1016/j.asr.2007.04.004

response of the lower atmosphere to a flare energy release is not restricted to the sites of propagation of the accelerated electrons (Kašparová et al., 2005a,b) but can be also associated with protons (Hénoux et al., 1990).

The recent simulations of particle acceleration in a 3D reconnecting current sheet (RCS) occurring on a top of the interacting loop structure have shown that electrons and protons can be accelerated to sub-relativistic energies and velocities within a very short timescale. Since electrons gain the velocities by 1–1.5 orders of magnitude higher than those by the protons then they can reach lower atmospheric levels under 1 s versus protons up to 20 s (Zharkova and Gordovskyy, 2004). Also, for some combinations of the 3D magnetic field components in an RCS suitable for solar flares, the protons and electrons can be fully or partially separated and ejected into the opposite legs of the reconnecting loop (Zharkova and Gordovskyy, 2004) as power law beams with the spectral indices varying from 1 to 10 (Zharkova and Gordovskyy, 2005a,b).

These high energy particles deposit their energy at all levels of a flaring atmosphere in Coulomb collisions, Ohmic dissipation and particle–wave interaction (Gordovskyy et al., 2005). During their participation these particle beams can lose the bulk of their energy in Coulomb collisions, Ohmic dissipation and dissipation on waves leading to different hydrodynamic responses caused by electrons or by protons (Zharkova and Zharkov, 2007).

However, at the lower chromospheric levels where the ambient plasma ionization is rather low, some part of the energy of beam electrons or protons can be deposited in non-thermal ionization and excitation of hydrogen and other neutral atoms the ambient plasma (Aboudarham and Henoux, 1986, 1987; Zharkova and Kobylinskii, 1991, 1993; Wulser et al., 1992).

Therefore, by comparing the observed temporal variations and spectra signatures of the brightening in H$\alpha$ line and in HXR emission for the event under investigation with those simulated from a combination of the kinetic, hydrodynamic and radiative models one can establish the scenario of particle and energy transport from the corona into lower chromospheric levels.

The observations of the flare used in the current paper are described in Section 2, the observations are compared with simulations and discussed in Section 3 and the conclusions are drawn in Section 4.

## 2. Description of the observations

The combined multi-wavelength investigation is very beneficial for understanding the mechanism of the energy release and transport into deeper atmospheric layers during the flaring event. For the analysis of this flare we use the following data: optical observations in the H$\alpha$ line from the Vacuum Tower Telescope (VTT), Observatorio del Teide, the line-of-sight (LOS) full-disk magnetograms provided by the SOHO (MDI) telescope, the EUV images from TRACE and the HXR data from RHESSI.

The M2.2 X-class flare presented in the paper occurred on the 25 July 2004 in the Active Region NOAA 10652; it started at 13:37 UT and ended at 13:55 UT, peaking at 13:49 UT. The HXR source images were reconstructed from the RHESSI observations for 12–25 and 25–50 keV bands by using the PIXON algorithm (Puetter and Pina, 1994; Metcalf et al., 1996).

In order to establish accurately the heliographic coordinates of the active region, we use the SOHO/MDI intensitygrams and TRACE images (195 and 1600 Å). The accuracy of the deduced heliographic coordinate is about 2″. The H$\alpha$ line slit-jaw images were taken in succession with a 5 s cadence for the chromospheric lines (H$\alpha$ and Ca II H) and whitelight. The duration of the whole series was usually about 1–2 min coveting the time interval 13:24:26–14:17:52 UT.

### 2.1. The temporal changes in H$\alpha$ emission and the HXR sources

For the observed period of time we obtained the difference images in H$\alpha$ intensity and searched for the locations of fast strong increases in intensity. The latter were found in the 10 bright kernels appeared at the following times: 1 – 13:38:38 UT; 2 – 13:38:44 UT; 3 – 13:38:49 UT; 4 – 13:38:55 UT; 5, 6, 7 – 13:40:06 UT; 8, 9 – 13:40:45 UT; 10 – 13:41:40 UT. After revealing the flare kernels a calibration of the processed images was carried out and the intensities averaged by the area for every flare kernel were obtained for the every moment of observations. The H$\alpha$ intensity variations in a few kernels are presented in Fig. 1 (bottom plot) revealing the three peaks in the intensity, the first one of lower intensity at about 13:39:00 UT for the kernels 1 and 3 or delayed by 10 and 20 s for the kernels 4 and 7 and the second one of much higher intensity appearing at 13:40.35 UT followed by the third one at 13:41:39 UT.

These fast changes of H$\alpha$ intensity occurring before the flare maximum correlate very closely with lower energy HXR emission (3–25 keV) observed by RHESSI (Fig. 1, upper plots). The increase of HXR emission started at 13:38:39 in lower energy bands (3–6, 6–12 and 12–25 keV) and the sharpest one is recorded in the 12–25 keV band. These energy bands allow to assume that the electron beams causing this emission were accelerated in a reconnection current sheet (RCS) of a moderate thickness formed by two interacting loops schematically drawn in Fig. 3 (Zharkova and Gordovskyy, 2004, 2005a). The absence of energy increase in higher energy bands is a good indication that there were no additional acceleration processes in this flare besides the acceleration by electric field generated during the magnetic reconnection. This provides a good environment for investigation of the consequences of the acceleration process onto the

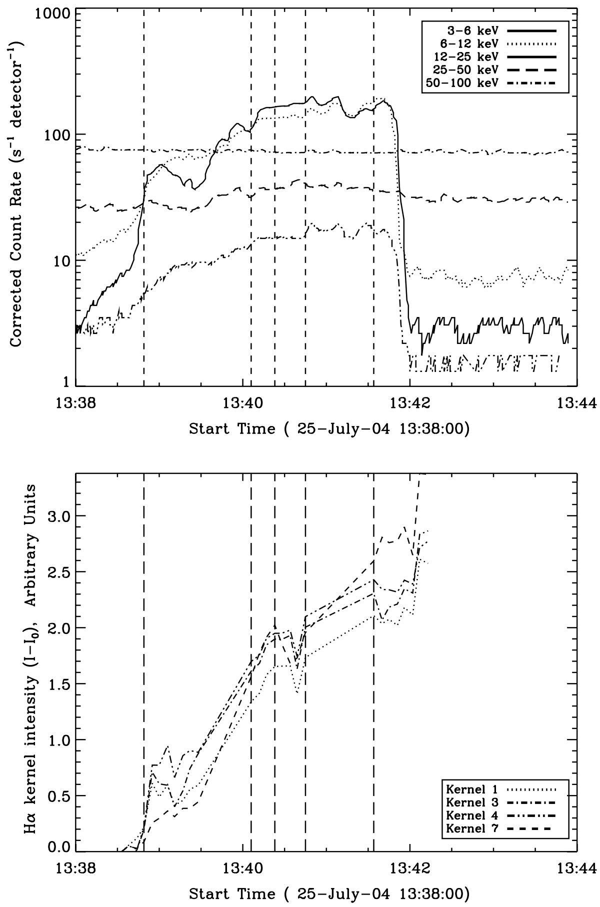


Fig. 1. Top: the temporal evolution of HXR photon spectra obtained from RHESSI. The dashed lines correspond to the events of fast rising of intensity on Hα images during the 25th July 2004 flare. Bottom: the temporal evolution of Hα intensity for different kernels in the locations shown in Fig. 2. Note that $I_0$ is the initial intensity of a kernel prior the flare onset.

signatures appeared during particle precipitation in the lower atmosphere.

### 2.2. The active region morphology with the locations of Hα emission kernels

The TRACE images with a higher spatial resolution taken from 13:38:49 UT to 13:41:04 UT (Fig. 2) are used to provide further information about the loops connectivity in the corona. The HXR sources contours and the ten Hα emission kernels are overplotted onto in Fig. 2 the TRACE images in 1600 and 195 Å (left and right panels, respectively). The HXR emission in the energy band of 12–25 keV is plotted by the dashed contours, in 25–50 keV by the solid contours, the inner ones correspond to 50% and outer one to 90% of the maximum intensity.

The TRACE loop structure was changing during the flare and at 13:41:38 UT, or 2 min later after the flare onset, it became rather complex (see the bottom panels) pointing out onto a number of interacting magnetic loops. The brightenings in the flaring region seen in the TRACE 1600 Å images are much higher than those in 195 Å. Although the area of brightening in 1600 Å is much higher and smoother than in 195 Å image, the loops in the latter were more complex and structured.

For the analysis of a magnetic field structure in this flare the SOHO/MDI magnetogram taken at 13:40:02 UT is used. The locations of Hα emission are shown in Fig. 4 on the magnetogram (left panel) and on the Hα line image (right panel). The detected Hα sources are located on the opposite sides from the location of an apparent magnetic neutral line (MNL, thereafter) that was approximately indicated by a dark filament seen in Hα images.

### 2.3. The electron beam parameters

The HXR photon light curves presented in Fig. 1 show a few phases of the HXR increase marked by the vertical dashed lines: the first one is the most steep one and a few others followed within a minute or two. This is likely to mark the initial impulsive injection of beam electrons followed by their steady injection within 2 min causing smaller spikes.

The photon energy spectra restored from the RHESSI measurements between 12 and 100 keV reveal well-defined double power law energy spectra with the lower spectral indices of four appearing at the energies of 12–40 keV and higher spectral indices of six at the energies of 50–100 keV (compare the third and fourth columns in Table 1). Moreover, the temporal variations of lower energy spectral indices show a clear soft–hard–soft pattern with the absolute magnitudes of the indices decreasing from 6.0 to 4.0 during the increase of the total photon flux and increasing back to six with the total photon flux decrease (compare the rows in the columns 2 and 3).

The spectra for the moments 2–4 are corrected for Ohmic losses in the self-induced electric field (Zharkova and Gordovskyy, 2006) with the turning points at 38–39 keV. This correction associated with the electron precipitation processes described by Zharkova and Gordovskyy (2006) allowed to change the absolute magnitudes of the spectral index for photon spectrum to six at all times. Also the temporal evolution of the total flux of the beam electrons is corrected from puzzling 'high–low–high' presented in column 3 of the Table 1 to the more physical one 'low–high–low' presented in column 4.

## 3. Comparison with the simulations

### 3.1. Non-LTE simulations of hydrogen emission

The temperature, density and macrovelocity variations plotted in Fig. 5 are calculated as hydrodynamic responses of a two-temperature plasma (electrons and ions) heated by the beam electrons and cooled by radiation by solving the continuity, momentum and two energy equations (for electrons and protons) (Somov et al., 1981; Zharkova and Zharkov, 2007).

For simulations of the heating function let us consider the beam electrons injected during the first impulsive phase

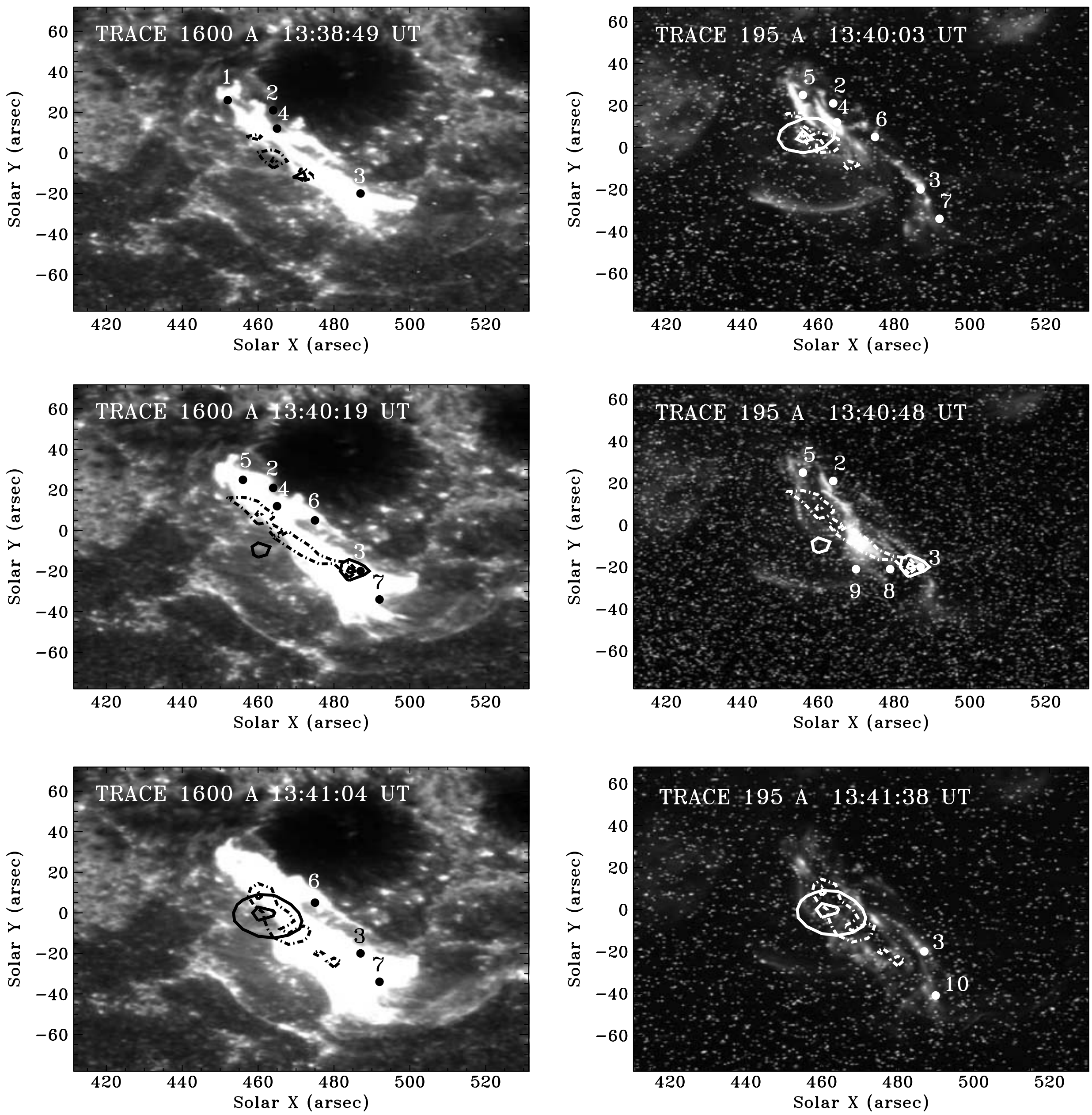


Fig. 2. The locations of the Hα emission kernels marked as black points and HXR sources overplotted on the TRACE images obtained in 195 and 1600 Å. The Hα emission kernel numbers correspond to their order of onset. The HXR sources are obtained for the 12–25 keV (dot–dash contours) and 25–50 keV bands (solid contours). The HXR sources are plotted as the contours (inner and outer ones) taken at the levels of 50% and 90%, respectively.

corresponding to the first spike of HXR emission marked by the most left vertical dashed line in Fig. 1. The duration of the first beam injection is assumed to be 10 s, the beam parameters are deduced from the RHESSI observation as discussed in Section 2.3, the initial energy flux is assumed to increase from lower to highest one in the first row of Table 1 and decreased back to lower during the flare time. The electron beam kinetics is computed by taking into account anisotropic scattering in collisions and Ohmic heating of ambient plasma particles with the temperature, density and macrovelocity profiles from Fig. 5. Then the heating caused by these beam electrons is calculated from these kinetic solutions as described in the paper by Gordovskyy et al. (2005).

The calculation of a radiative cooling includes the radiative losses in optically thin plasma with the coronal abundance (Cox and Tucker, 1969) and, in addition, the energy losses in optically thick hydrogen lines and continua (Kobylinskij and Zharkova, 1996). The full Hα intensity integrated within the Hα line wavelength, (Fig. 6, solid lines) as well as the intensities in all other hydrogen lines and continua are calculated from the full non-LTE approach. A 5 levels plus continuum hydrogen atom is considered taking into account radiative, thermal and

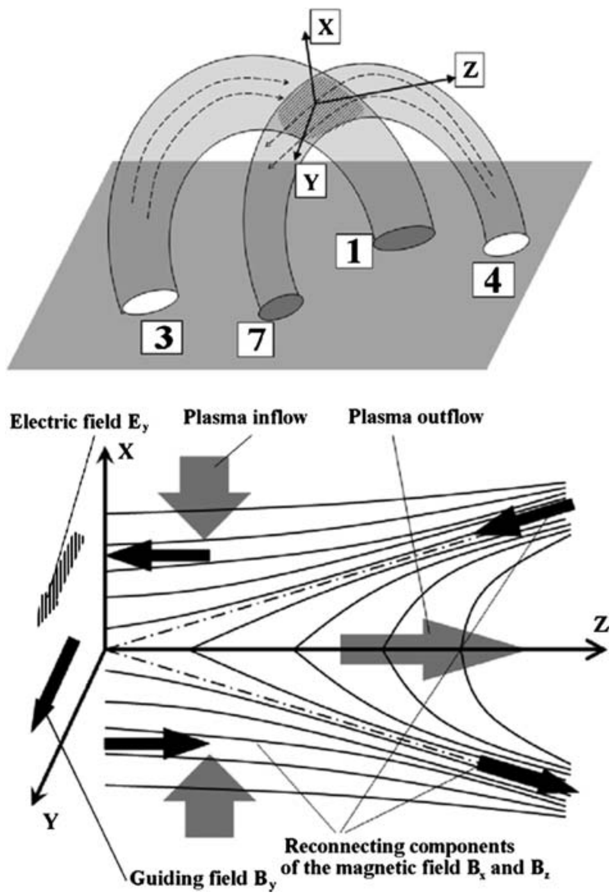


Fig. 3. 3D model of a magnetic reconnection of the two interacting loops (upper plot) and a 3D RCS occurring on the top. The numbers at the footpoints denote assumed locations of the Hα kernels connecting one loop (1–3) and the other one (4–7).

non-thermal excitation and ionization processes as described in the paper by Zharkova and Kobylinskii (1993).

During the first 10 s of the beam injection the theoretical hydrodynamic models show a moderate increase of a temperature and density at the chromospheric levels (see Fig. 5) that cannot account for the observed increase of the hydrogen emission in many kernels reported above. Only, if non-thermal excitation and ionization by beam electrons is taken into account, the first peak in Hα emission appears simultaneously (within 5 s) with HXR emission. Much brighter Hα emission observed later during the gradual phase (after 10 s onwards) can be explained by the hydrodynamic heating developed after the impulsive beam ejection is switched off.

Indeed, the non-LTE simulations of hydrogen emission taking into account the non-thermal hydrogen excitation and ionization by beam electrons reveal that immediately after the electron beam injection there is a sharp increase of the Hα emission caused by these high energy electrons (the impulsive phase). A further increase in the Hα intensity occurs owing to a fast thermo-conductive heating in the hydrodynamic response to the electron beam injection that was reported in many other similar simulations (Somov et al., 1981; Fisher et al., 1985; Wulser and Marti, 1989).

The theoretical curve calculated for the beam electrons with the parameters taken from Section 2.3 are plotted in Fig. 6 versus the observed evolution of the Hα kernels 1 and 3 and 4 and 7. The temporal profile of the observed Hα emission in the kernel 1 and kernel 3 starting at 13:38:49 UT fit qualitatively rather well the theoretical emission increase in the impulsive phase caused by an electron beam with the derived parameters. In the kernels 4 and 7 the observed Hα emission appears with a delay of about 10–30 s comparing to the theoretical Hα maxima caused by the electron beam. Neither of these kernels have any HXR emission in spite the kernel 7 is located rather close to kernel 3 and the HXR source. Also the polarity of a magnetic field in the kernel 7 is opposite to those in the kernel 3.

### 3.2. General discussion

The temporal and spatial locations of the HXR emission and the Hα brightening in the 10 kernels indicate that in this set of loops there were numerous magnetic reconnections (MRs) occurring in a succession between the interacting loops connecting the Hα kernels from the north-west locations to those in the south-east one to form two ribbons from the both sides from MNL. Moreover, from a comparison of the locations of the kernels 1 and 4 occurring on the north-west side from the MNL and 3 and 7 occurring on the opposite (south-east) side from the MNL, it is possible to assume that they are the parts of the two interacting loops. This, in turn, points out to the legs of these interacting loops being embedded into the photosphere in the footpoints 1, 3, 4 and 7 as schematically marked in Fig. 3.

Since the kernel 3 was spatially and temporarily rather close to the observed HXR location and times (see Fig. 4), this allows to assume that only electrons can produce this correlation. Then, according to the particle acceleration model (Zharkova and Gordovskyy, 2004), the same should be valid for other footpoint of this loop, the kernel 1.

The absence of HXR emission in the kernel 1 can be explained by the suggestion that the reconnection site occurred much closer to the kernel 3 than to the kernel 1. Hence, the electrons had much shorter path to and precipitated to much deeper atmosphere in the kernel 3 while they would have a much longer path to the footpoint in the kernel 1. The observations show there was no HXR emission observed higher than 100 keV that defines the maximum energy of beam electrons injected in these loops. Therefore, on their precipitation into the footpoint 1 electrons would travel much longer and become subject not only collisional but Ohmic losses that could turn them backwards to the source (Zharkova and Gordovskyy, 2006). This can explain why their path is seen as an extended HXR source on the line connecting the kernels 1 and 3 that never reaches the location of kernel 1.

The kernels 4 and 7 show a delay of 20–30 s in the appearance of Hα brightenings comparing to the HXR

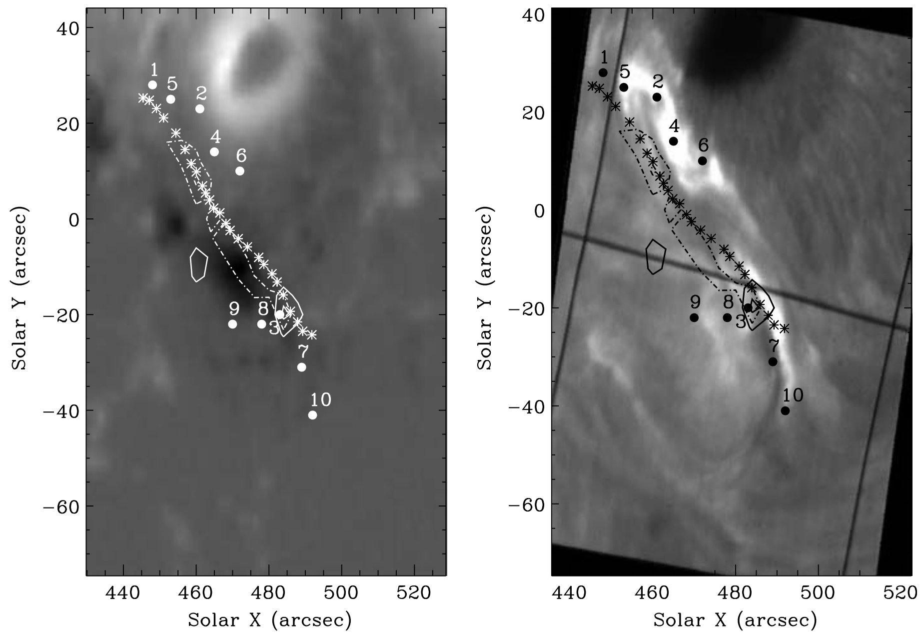


Fig. 4. The SOHO/MDI magnetogram taken at 13:40:02 UT (the left panel) and Hα-line image at 13:40:45 UT (the right panel). The locations of the Hα emission (kernels) marked by white dots on the left panel and by the black dots on right one. The HXR sources are overplotted on the images as contours taken at the levels of 50% and 90% of their maximum intensity in 12–25 keV (dot–dashed contours) and 25–50 keV bands (solid contours). The magnetic polarity inversion line, or magnetic neutral line (MNL), derived from the filament location is shown by the asterisks.

Table 1
The temporal evolution of the HXR photon spectra: time (the first column), spectral indices in the lower energy range of 12–39 keV (the second column) and total fluxes before (the third column) and after the correction for Ohmic losses in the self-induced electric field (Zharkova and Gordovskyy, 2006) (the fourth column)

| Time (UT) | Spectral index | Total flux (erg/cm$^2$s$^{-1}$) | Corrected total flux (erg/cm$^2$s$^{-1}$) |
|---|---|---|---|
| 13:39:49–13:39:53 | −6.02 | $2.64 \times 10^{10}$ | $2.64 \times 10^{10}$ |
| 13:40:13–13:40:17 | −4.91 | $1.43 \times 10^{10}$ | $6.69 \times 10^{10}$ |
| 13:40:38–13:40:42 | −4.06 | $5.04 \times 10^{9}$ | $9.60 \times 10^{10}$ |
| 13:41:08–13:41:12 | −4.79 | $2.50 \times 10^{10}$ | $8.44 \times 10^{10}$ |
| 13:41:38–13:41:42 | −4.22 | $4.37 \times 10^{10}$ | $5.26 \times 10^{10}$ |

For the higher energy range of 39–100 keV the photon spectral index was −6.02 for all the moments.

in the kernels 1 and 3 that points out onto some other agents causing these brightenings. These agents can be either thermal neutral fluxes or beam protons that precipitate into this second loop reconnecting with the first loop that links the kernels 1–3. However, thermal fluxes would travel much longer than the delay of maximum 20 s observed.

This, in turn, lends a very strong support to the model for particle acceleration in a reconnecting current sheet with the separation of proton from electron beams into the opposite loop legs as shown in Fig. 3 and described by Zharkova and Gordovskyy (2004, 2005a,b). The confirmation of this assumption is also contained in the temporal delays in Hα emission in the 4–7 kernels comparing to those in 1–3 ones with the delay time about of 10–30 s that fits surprisingly well the theoretical predictions of Hα emission (Fig. 6). It has to be noted that without non-thermal excitation and ionization, the current peak appearing just before 13:39 UT in the integrated Hα line intensity would disappear, the Hα emission would start from zero and after 13:39 UT increase to a magnitude marked by the solid line that is likely to be caused by a hydrodynamic heating.

## 4. Conclusions

In the present paper the Hα brightening obtained by VTT were investigated in the solar flare of 25 July 2004 simultaneously with HXR emission from RHESSI, and EUV images from TRACE. Based on the observational and numerical results presented above we can conclude:

(1) In this flare there are a few phases of the HXR increase reflecting the initial impulsive injection of beam electrons followed within 2 min by more steady injection with smaller spikes. HXR emission was observed only in the 12–25 and 25–50 keV bands.
(2) The HXR photon energy spectra have shown a strong flattening at lower energies (double power laws) caused by a self-induced electric field that became stronger during the flare maximum (a soft–hard–soft temporal evolution).

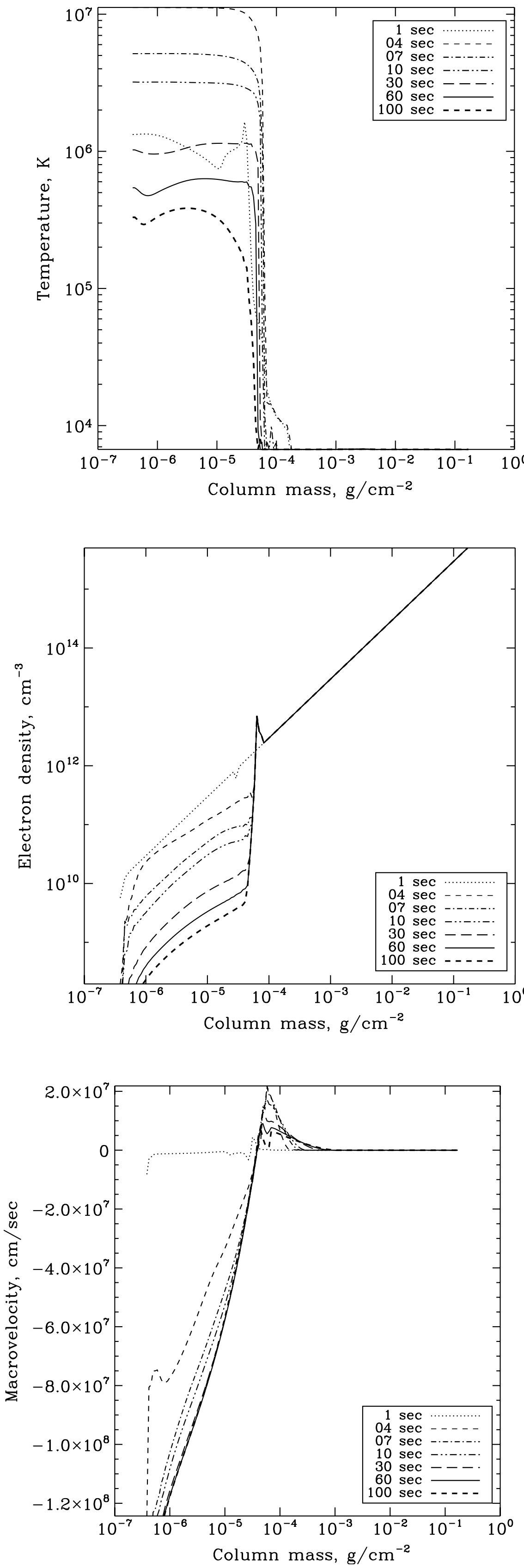


Fig. 5. The temperature, density and macrovelocity variations calculated from a hydrodynamic response to the injection of an electron beam with parameters from the Table 1.

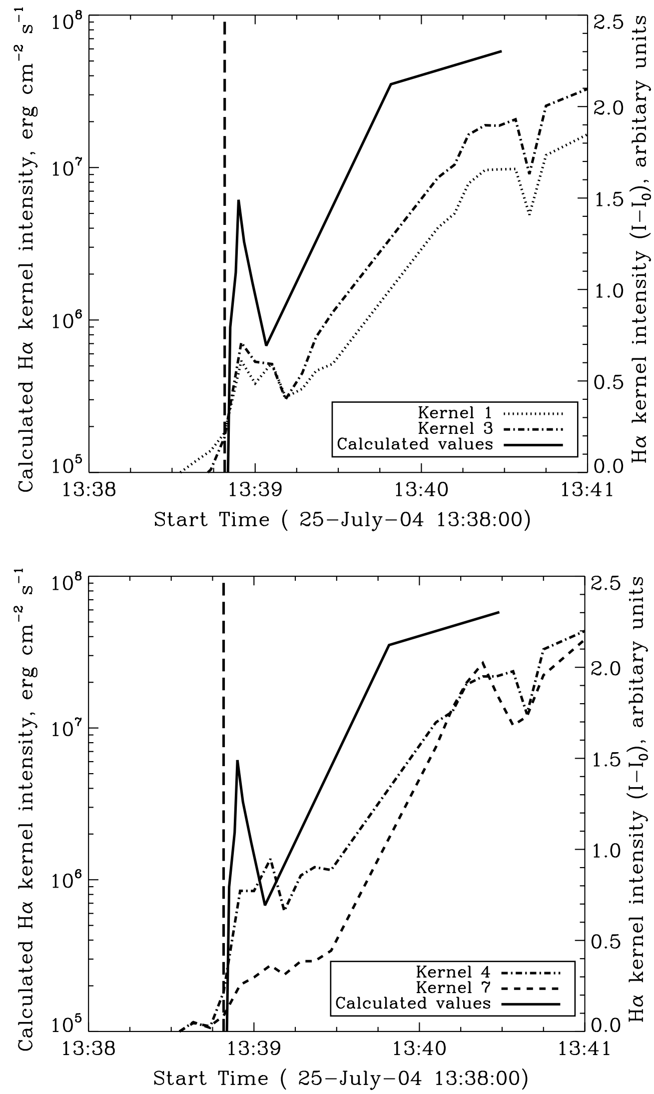


Fig. 6. The temporal variations of the full integrated in Hα line intensity simulated for the atmosphere heated by the electron beam with the parameters from Table 1 (solid curve) and those observed in the electron dominated kernels (1 and 3) (the upper plots) and in the proton dominated kernels (4 and 7) (the lower plots).

(3) There are also 10 Hα kernels appeared either simultaneously with the HXR emission (1, 2 and 3) or delayed by 10–60 s (4–10).
(4) The locations of HXR and Hα sources towards the magnetic neutral line in this flare point out onto a two ribbon flare with the Hα sources appearing in the locations where loops are embedded into the photosphere. The connection is suggested for the kernels 1 and 3 (first loop) and 4 and 7 (second loop).
(5) The appearance of the HXR sources only on one side from the magnetic neutral line and their elongation along the line connecting the kernels 1 and 3 points out to high energy electrons precipitating into this first loop while according to the theoretical model (Zharkova and Gordovskyy, 2004) protons should be precipitating into the second loop.

(6) The theoretical hydrodynamic models calculated for the first seconds of the beam injection show a moderate increase of temperature and density at the chromospheric levels that cannot account for an increase of hydrogen emission in the Hα line.
(7) However, if the non-thermal excitation and ionization is taken into account this can explain the first peak in Hα emission in the electron-activated kernels (1 and 3). Also a hydrodynamic heating caused by beam electrons can account for the gradual phase in Hα emission.
(8) The other Hα kernels (4 and 7) showing a delay of 10–30 s in the appearance of Hα brightening are likely to confirm that there are the other agents, protons, precipitating into this second loop reconnecting with the first one where electrons precipitate.

These results lend a very strong support to the model for particle acceleration in a reconnecting current sheet with the separation of proton from electron beams into the opposite loop legs (Zharkova and Gordovskyy, 2004).

## Acknowledgements

L.K., S.C. and V.Z. thank the Royal Society, UK for supporting this research with two short visit grants for L.K. and S.C., L.K. and S.C. also thank the University of Bradford for the hospitality and facilities provided during these visits that accelerated enormously the paper progress. We thank E.V. Khomenko and S.N. Osipov for their participation in the VTT observations. The research by S.C. was supported by the grant of the National Academy of Science of Ukraine.

## References

Aboudarham, J., Henoux, J.C. Non-thermal excitation and ionization of hydrogen in solar flares. I – effects on a flaring chromosphere. Astronomy and Astrophysics 168, 301–307, 1986.

Aboudarham, J., Henoux, J.C. Non-thermal excitation and ionization of hydrogen in solar flares. II – effects on the temperature minimum region energy balance and white light flares. Astronomy and Astrophysics 174, 270–274, 1987.

Asai, A., Masuda, S., Yokoyama, T., et al. Difference between spatial distributions of the Hα kernels and hard X-ray sources in a solar flare. The Astrophysical Journal 578, L91–L94, 2002.

Cox, D.P., Tucker, W.H. Ionization equilibrium and radiative cooling of a low-density plasma. The Astrophysical Journal 157, 1157–1167, 1969.

Fisher, G.H., Canfield, R.C., McClymont, A.N. Flare loop radiative hydrodynamics – part six – chromospheric evaporation due to heating by nonthermal electrons. The Astrophysical Journal 289, 425–433, 1985.

Gordovskyy, M., Zharkova, V.V., Voitenko, Yu.M., Goossens, M. Proton versus electron heating in solar flares. Advances in Space Research 35, 1033–1047, 2005.

Heinzel, P. Understanding solar flares from optical observations: how do particle beams affect the lower atmosphere? Advances in Space Research 32, 2393–2402, 2003.

Hénoux, J.C., Chambe, G., Smith, D., et al. Impact line linear polarization as a diagnostic of 100 keV proton acceleration in solar flares. The Astrophysical Journal, Supplement Series 73, 303–311, 1990.

Kašparová, J., Karlický, M., Kontar, E.P., Schwartz, R.A., Dennis, B.R. Multi-wavelength analysis of high-energy electrons in solar flares: a case study of the august 20, 2002 flare. Solar Physics 232, 63–86, 2005a.

Kašparová, J., Karlický, M., Schwartz, R.A., Dennis, B.R. X-ray and Hα emission of the 20 Aug 2002 flare, in: Hanslmeier, A., Veronig, A., Messerotti, M. (Eds.), Solar Magnetic Phenomena, Proceedings of the 3rd Summerschool and Workshop held at the Solar Observatory Kanzelhöhe, Kärnten, Austria, August 25–September 5, 2003. Astronomy and Astrophysics Space Science Library, 320, Springer, Dordrecht, The Netherlands, pp.187–190, 2005b.

Kobylinskij, V.A., Zharkova, V.V. Hydrogen emission and radiative losses in the impulsive solar events. Advances in Space Research 17 (4–5), 110–114, 1996.

Metcalf, T.R., Hudson, H.S., Kosugi, T., et al. Pixon-based multiresolution image reconstruction for Yohkoh's hard X-ray telescope. The Astrophysical Journal 466, 585–594, 1996.

Puetter, R.C., Pina, R.K. Beyond maximum entropy: fractal pixon-based image reconstruction. Experimental Astronomy 3, 293–296, 1994.

Somov, B.V., Spektor, A.R., Syrovatskii, S.I. Hydrodynamic response of the solar chromosphere to an elementary flare burst. I – heating by accelerated electrons. Solar Physics 73, 145–155, 1981.

Trottet, G., Rolli, E., Magun, A., et al. The fast and slow Halpha chromospheric responses to non-thermal particles produced during the 1991 March 13 hard X-ray/gamma-ray flare at 08 UTC. Astronomy and Astrophysics 356, 1067–1075, 2000.

Wulser, J.P., Marti, H. High time resolution observations of H alpha line profiles during the impulsive phase of a solar flare. The Astrophysical Journal 341, 1088–1096, 1989.

Wulser, J.P., Canfield, R.C., Zarro, D.M. Energetics and dynamics in a large solar flare of 1989 March. The Astrophysical Journal 384, 341–347, 1992.

Zharkova, V.V., Gordovskyy, M. Particle acceleration asymmetry in a reconnecting nonneutral current sheet. The Astrophysical Journal 604, 884–8914, 2004.

Zharkova, V.V., Gordovskyy, M. Energy spectra of particles accelerated in a reconnecting current sheet with the guiding magnetic field. Monthly Notices of the Royal Astronomical Society 356, 1107–1116, 2005a.

Zharkova, V.V., Gordovskyy, M. The kinetic effects of electron beam precipitation and resulting hard X-ray intensity in solar flares. Astronomy and Astrophysics 432, 1033–1047, 2005b.

Zharkova, V.V., Gordovskyy, M. The Effect of a self-induced electric field on hard X-ray photon and electron spectra in solar flares. The Astrophysical Journal 651, 553, 2006.

Zharkova, V.V., Kobylinskii, V.A. Investigation of nonthermal excitation and ionization of hydrogen in low-temperature flare plasma – part two – computational method. Soviet Astronomy Letters 17, 34–38, 1991.

Zharkova, V.V., Kobylinskii, V.A. The effect of non-thermal excitation and ionization on the hydrogen emission in impulsive solar flares. Solar Physics 143, 259–274, 1993.

Zharkova, V.V., Zharkov, S. On the origin of seismic sources associated with the flare 28 October 2003. The Astrophysical Journal 664 (2), 2007.